Intelligent control of Induction Motor integrated with PV Micro Inverter using ANFIS

Gunasekaran.M[1]

[1]*Assistant Professor/EEE & Annapoorana Engineering College*

---***---

Abstract— This paper presents a boost-half-bridge Photovoltaic (PV) micro inverter system and its control implementations over single phase induction motor. In order to achieve low cost, easy control, high efficiency, and high reliability, a boost-half-bridge dc–dc converter using minimal devices is introduced to interface the low-voltage PV module. A full-bridge pulse width-modulated inverter is cascaded and injects synchronized sinusoidal current to the single phase induction motor. Moreover, a plug-in repetitive current controller based on a fourth-order linear phase IIR filter is proposed to regulate the single phase induction motor current using ANFSI. High power factor and very low total harmonic distortions are guaranteed under both heavy load and light load conditions. Dynamic stiffness is achieved when load or solar irradiance is changing rapidly. In addition, the dynamic behavior of the boost-half-bridge dc–dc converter is analyzed; a customized maximum power point tracking (MPPT) method, which generates a ramp-changed PV voltage reference is developed accordingly by the help of ANFSI. Variable step size is adopted such that both the fast tracking speed and high MPPT efficiency are obtained.

Simulation results are provided to verify the validity and performance of the circuit operations, current control, and MPPT algorithm of ANFSI.

Keywords—**ANFSI, Boost-half-bridge, maximum power point tracking (MPPT), Photovoltaic micro inverter, repetitive current control.**

INTRODUCTION

With economic development and social progress, the energy demand increases gradually and routine sources of energy demand exceeds supply. The solar energy is one kind of the new sources of energy having a potential. Photovoltaic (PV) system commonly used batteries as energy storage components, requiring the use of photovoltaic chargers to charge. But the photovoltaic array has the strong non-linear relationship with intensity of sunshine, solar cell surface temperature and other factors, resulting in a battery terminal voltage will change with the external environment. So this charge cannot always guarantee that it will be in the vicinity solar maximum power point, which caused a waste of resources. In order to achieve maximum power point tracking (MPPT), both at home and abroad put forward a number of methods. The concept of micro inverter (also known as module integrated converter/inverter) has become a future trend for single-phase Induction motor-connected photovoltaic (PV) power systems for its removal of energy yield mismatches among PV modules, possibility of individual PV-module-oriented optimal design, independent maximum power point tracking (MPPT), and "plug and play" concept. In general, a PV micro inverter system is often supplied by a low-voltage solar panel, which requires a high-voltage step-up ratio to produce desired output ac voltage. Hence, a dc–dc converter cascaded by an inverter is the most popular topology, in which a HF transformer is often implemented within the dc–dc conversion stage [1].Through the previous experiment, we can see, MPPT will enable the output power increased by about 15% -36%. Commonly used methods are the constant voltage tracking method that based an optimized mathematical model, the perturb and observe algorithm and the incremental conductance algorithm that based on the disturbed self-optimizing. Including the neural network and ANFIS control are based on the artificial intelligence. Modern control system is highly complex, when it is difficult to accurately determine the mathematical model of a control object, or the state of the information obtained from object is extremely vague and lacking, the traditional control strategy is often difficult to meet the system dynamic and static characteristics height requirements, ANFIS logic has become a powerful tool. As the non-linear characteristics, the output power of PV system varies with the working conditions. In order to obtain better control of maximum power point tracking results, it will adjust MPPT circuit disturbance step based on the external environment.
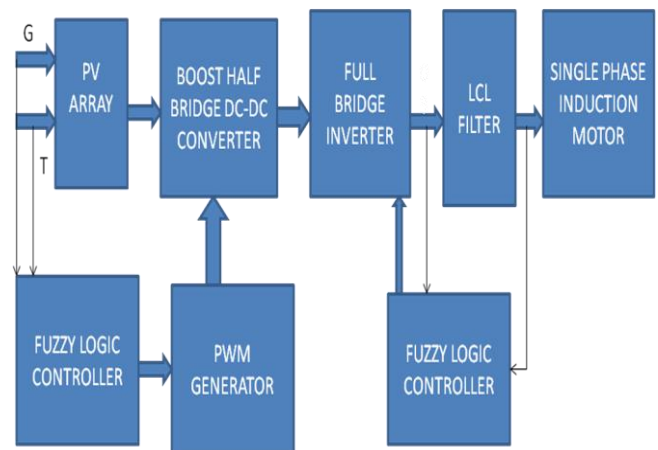
solar cell I-V characteristic

FIGURE 1: **Block diagram of proposed system**

Typically, an undamped *LCL* filter exhibits a sharp *LC* resonance peak, which indicates a potential stability issue for the current regulator design. Hence, either passive damping or active damping techniques can be adopted to attenuate the resonance peak below 0 dB . On the other hand, a current regulator without introducing any damping method can also be stabilized, as long as the *LCL* parameters and the current sensor location are properly selected . In this paper, the *LCL* parameters are selected . The current sensor is placed at the inverter side instead of the grid side. Resultantly, no damping techniques are needed such that the current control is much simplified.

The solar cell I-V characteristic is shown in FIGURE 2. is the characteristic curve of the load and Pmax is under different environmental conditions of maximum power point of the curve synthesis. When environmental conditions change in the outside world, it is necessary to change the load so that the photovoltaic system will reach the maximum power output under any conditions.
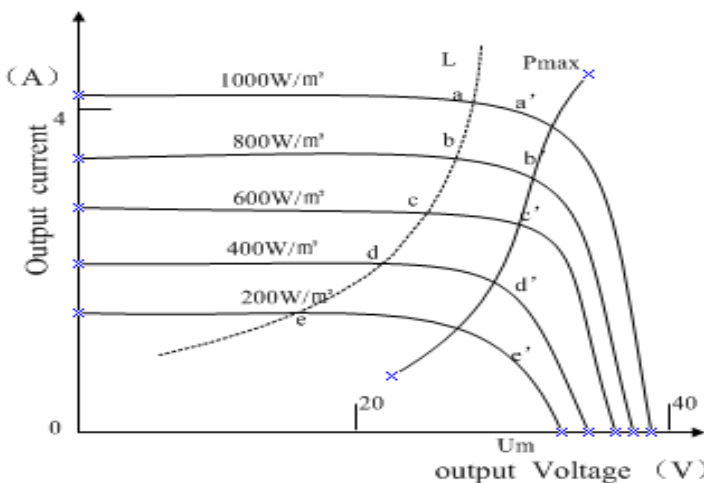

FIGURE 2: V-I characteristics

the boost-half-bridge micro inverter topology for single phase induction motor connected PV systems

A. Construction

In the FIGURE.3, the boost-half-bridge micro inverter topology for single phase induction motor connected PV systems is depicted. It is composed of two decoupled power processing stages. In the front-end dc–dc converter, a conventional boost converter is modified by splitting the output dc capacitor into two separate ones. Cin and Lin denote the input capacitor and boost inductor, respectively. The center taps of the two MOSFETs (S_1 and S2) and the two output capacitors (C_1 and C_2) are connected to the primary terminals of the transformer T_r, just similar to a half bridge. The transformer leakage inductance reflected to the primary is represented by Ls and the transformer turns ratio is 1: n. A voltage doubler composed of two diodes (D_1 and D_2) and two

capacitors (C_3 and C_4) is incorporated to rectify the transformer secondary voltage to the inverter dc link. A full-bridge inverter composed of four MOSFETs (S_3–S_6) using synchronized PWM control serves as the dc–ac conversion stage. Sinusoidal current with a unity power factor is supplied to the single phase induction motor through a third-order LCL filter (L_{o1}, L_{o2}, and C_o). Other symbol representations are defined as follows. The duty cycle of S_1 is denoted by d_1. The switching period of the boost half-bridge converter is T_{sw1}. The PV current and voltage are represented by iPV and vPV, respectively. The voltages across C_1, C_2, C_3, and C_4 are denoted by v_{c1}, v_{c2}, v_{c3} and v_{c4} respectively. The transformer primary voltage, secondary voltage, and primary current are denoted as v_{r1}, v_{r2} and i_{r1} respectively. The low-voltage side (LVS) dc-link voltage is vdc1 and the high voltage side (HVS) dc-link voltage is v_{dc2}. The switching period of the full bridge inverter is T_{sw2}. The output ac currents at the inverter side and the single phase induction motor side are represented by i_{inv} and i_g, respectively. The single phase induction motor voltage is v_g. The boost-half-bridge converter is controlled by S_1 and S_2 with complementary duty cycles. Neglect all the switching dead bands for 1simplification. The idealized transformer operating waveforms are illustrated in Fig. 4.2.
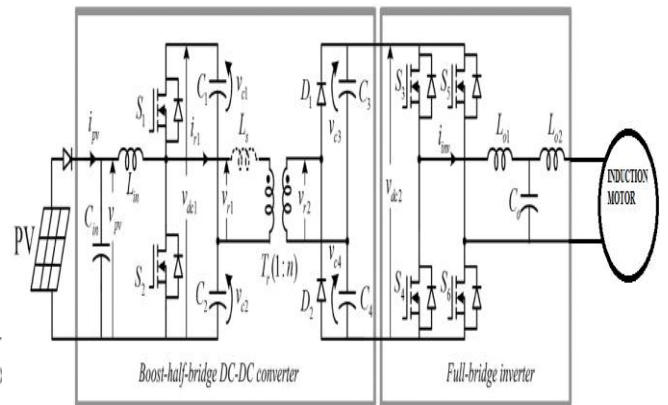
Topology of the boost-half-bridge PV microinverter.

FIGURE 3: **Circuit diagram of proposed system**

B. Operation

When S_1 is ON and S_2 is OFF, v_{r1} equals to v_{c1}. When S_1 is OFF and S_2 is ON, v_{r1} equals to $-v_{c2}$. At the steady state, the transformer volt-second is always automatically balanced. In other words, the primary volt-second A_1 (positive section) and A_2 (negative section) are equal, so are the secondary volt-sec A_3 (positive section) and A_4 (negative section). Normally, D_1 and D_2 are ON and OFF in a similar manner as S_1 and S_2, but with a phase delay tpd due to the transformer leakage inductance. Ideally, the transformer current waveform is determined by the relationships of $v_{c1}-v_{c4}$, the leakage inductance L_s , the phase delay t_{pd}, and S_1 's turn-ON time $d_1 T_{sw1}$ [1]. In order to reach an optimal efficiency of the boost-half-bridge converter, ZVS techniques can be

considered for practical implementation, as guided by [1]. It is worth noting that engineering tradeoffs must be made between the reduced switching losses and increased conduction losses when soft switching is adopted. Detailed optimal design processes of the boost-half-bridge converter will not be addressed in this paper.
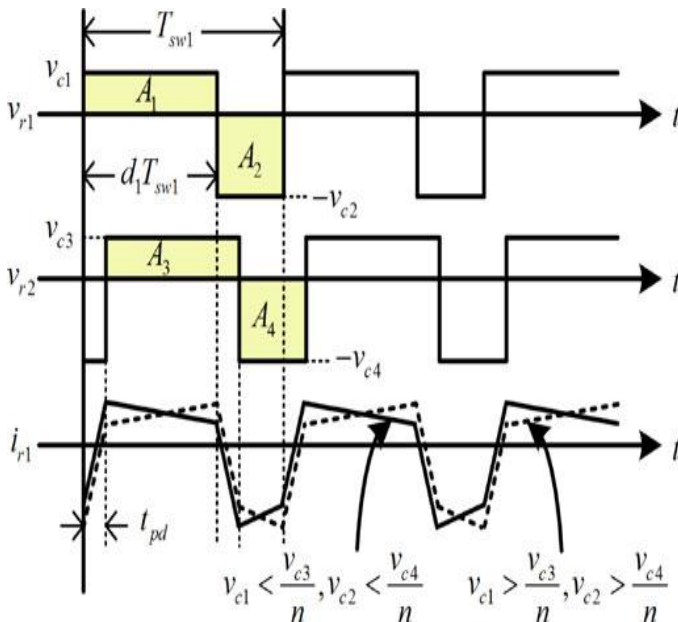

FIGURE 4: Idealized transformer voltage and current.

For simplicity, hard switching is employed and the transformer leakage inductance is regarded as small enough in this paper. Therefore, (1) and (2) can be derived as follows:

$$V_{c1} = \frac{(1-d_1)}{d_1} V_{PV} \quad V_{c2} = V_{PV} \quad V_{c1} = \frac{V_{PV}}{d_1} \qquad (1)$$

$$V_{c3} = \frac{n(1-d_1)}{d1} V_{PV} \quad V_{c4} = nV_{PV} \quad V_{dc2} = \frac{nV_{PV}}{d_1} \qquad (2)$$

When viewing from the full-bridge inverter, the boost-half bridge converter just operates identically as a conventional boost converter, but with the extra features of the galvanic isolation as well as the high step-up ratio.

C. Design of controller

An all-digital approach is adopted for the control of the boost half- bridge PV micro inverter system. The PV voltage v_{PV} and current i_{PV} are both sensed for calculation of the instantaneous PV power P_{PV}, the PV power variation ΔP_{PV}, and the PV voltage variation Δv_{PV}. The MPPT function block generates a reference $v*_{PV}$ for the inner loop of the PV voltage regulation, which is performed by the dc–dc converter. At the inverter side, the single phase induction motor voltage v_g is sensed to extract the instantaneous sinusoidal angle θ_g, which is commonly known as the phase

lock loop. The inverter output current i_{inv} is pre filtered by a first-order low-pass filter on the sensing circuitry to eliminate the HF noises. The filter output $i*_{inv}$ is then fed back to the plug-in repetitive controller for the inner loop regulation. Either v_{dc1} or v_{dc2} can be sensed for the dc-link voltage regulation as the outer loop. In practice, the LVS dc-link voltage v_{dc1} is regulated for cost effectiveness. The single phase induction motor current and the LVS dc-link voltage references are represented by $i*_{inv}$ and $v*_{dc1}$, respectively.

In order to achieve fast dynamic responses of the single phase induction motor current as well as the dc-link voltage, a current reference feed forward is added in correspondence to the input PV power P_{PV}. The magnitude of the current feed forward is expressed as follows:

$$\left| i_{inv} \right| ff = \frac{2P_{PV}}{|v_g|} \qquad (3)$$ where

$|v_g|$ is the magnitude of the single phase induction motor voltage and can be calculated

by $$|v_g| = \frac{1}{2} \int_0^\pi v_g d\theta_g \qquad (4)$$

D. Design Considerations:

Equations (1) and (2) indicate that v_{c1}–v_{c4} are changing dynamically in accordance with d_1. It is worth noting that the charge and discharge of C_1–C_4 caused by the uneven voltage distribution on the upper capacitors (C_1 and C_3) and the lower capacitors (C_2 and C_4) can only be conducted through the transformer magnetizing inductor. As a result, at any time, the charge and discharge rate of C_1–C_4 must be limited such that the transformer flux is not saturated. Intuitively, this can be done by either introducing the transformer flux as a state variable into the inner PV voltage regulator or designing the outer MPPT block adaptively. For the sake of control simplicity and low cost, developing a customized MPPT method by carefully taking care of the boost-half-bridge converter dynamics would be more desirable.

E. Dynamics of the Boost-Half-Bridge Converter

As previously discussed, the boost-half-bridge converter can be regarded as the integration of two sub circuit topologies: 1) the boost converter and 2) the half-bridge converter. The PV voltage regulator depicted in Fig. 8 has ensured that both the steady state and the dynamic response of the boost converter part are taken care of. Hence, the following analysis will be only concentrated on the dynamics of the half-bridge converter part. The major role of the half-bridge converter here is to transfer energy from the LVS dc link to the HVS dc link through the transformer. But besides that, it also allocates the amount of stored charges on the upper dc-link capacitors (C_1 and C_3) and the lower dc-link capacitors (C_2 and C_4). Neglecting the effect of the transformer leakage inductance and power losses at this

time, it depicts the extracted half bridge converter part and its equivalent circuit seen from the LVS dc link. As v_{dc1} is regulated to a constant dc, the LVS dc link is simply connected to a constant voltage source for approximation. C_3 and C_4 are both reflected to the transformer primary and combined with C_1 and C_2. C_1 and C_2 stand for the equivalent dc-link capacitors, where $C_1 = C_1 + n_2C_3$ and $C_2 = C_2 + n_2C_4$. L_m, i_m, and λ_m denote the transformer primary magnetizing inductor, dc current and dc flux linkage respectively.

At the steady state, both i_m and λ_m are zero. But once the converter duty cycle d_1 is perturbed, i_m and λ_m will increase or decrease such that the electric charges can be transferred from C_1 to C_2 or vice versa. According to the Faraday's law, one has

$$v_{c1}(t)d_1(t) - v_{c2}(t)(1-d_1(t)) = \frac{d\lambda_m(t)}{dt} \quad (5)$$

Define the duty cycle change rate $d_1(t) = d(d_1(t))/dt$. Take derivative on both sides of (5), then

$$v_{dc1}(t)\,d'_{11}(t) - \frac{dv_{c2}(t)}{dt} = \frac{d\lambda_m(t)}{dt} \quad (6)$$

Furthermore, the capacitor charge and discharge equation can be expressed as follows:

$$(C'_1 + C'_2)\frac{dv_{c2}(t)}{dt} = i_m(t) = \frac{\lambda_m(t)}{L_m} \quad (7)$$

Plug (7) into (6), then

$$\frac{d\lambda_m(t)}{dt} + \frac{\lambda_m(t)}{L_m(C'_1 + C'_2)} - v_{dc1}(t)d'_{11}(t) = 0 \quad (8)$$

Equation (8) describes the dynamics of a typical second-order system, where $d_1(t)$ is the excitation and $\lambda_m(t)$ is the response. If d_1 is constant initially (at the steady state) and then perturbed by the MPPT operation, λ_m will start to oscillate with a frequency of $1/(2\pi\_L_m(C_1 + C_2))$.

Defining the magnitude of λ_m as $|\lambda_m|$ and assuming

$$|\lambda m| = 2v_{dc1}L_m(C'_1 + C'_2)\,d'_1 \quad (9)$$

Assume that $|\lambda_m|max$ is the maximum permissible flux linkage in the transformer for avoidance of the magnetic saturation, then the constraint for the duty cycle change rate is given by

$$d'_1 < \frac{|\lambda_m|_{max}}{2v_{dc1}L_m(C'_1 + C'_2)} \quad (10)$$

1. MPPT with a Ramp-Changed Voltage Reference

Generally speaking, L_m and $(C_1 + C_2)$ are relatively large because of the high permeability of the transformer core and the required energy storage capability of the dc-link capacitors to absorb the double-line-frequency power ripple. Therefore, the constraint given by (10) can hardly be satisfied if an MPPT method that produces a step-changed voltage reference is implemented. In order to strictly follow a customized MPPT method that periodically generates a ramp-changed voltage reference is developed in this paper. Applying the system control provided in Fig. 3, the simulation results of the boost-half-bridge converter are depicted in Fig. 5.2. The step-changed voltage reference and the ramp-changed voltage reference are implemented for MPPT, respectively. Transformer leakage inductance and power losses are both taken into account in the simulation. From Fig. 10, it is noticeable that λ_m has an average of zero with the double-line-frequency ripple when the PV voltage is constant. An oscillation of λ_m occurs once the PV voltage is perturbed by the MPPT operation. The slope of the voltage ramp in Fig. 5.2(b) is chosen in consistency with (10). Here, the MPPT step size is selected as 0.3V. The time duration of the voltage ramp in Fig. 5.2(b) is denoted by t_{rp}. In this paper, $t_{rp} = 75$ ms. One can clearly see that with the ramp-changed voltage reference, the transformer flux linkage is well confined within the permissible range.

2. Variable Step-Size MPPT Algorithm

For simplicity, it is assumed that the PV module is working under the standard irradiance (1000 W/m2) and the room temperature (25oC).

FIGURE 5, Efficiency chart of the boost-half-bridge dc–dc converter. Then, dP_{PV}/dv_{PV} is illustrated. It is worth mentioning that some MPPT techniques calculate the step size online relying on the instantaneous values of ΔP_{PV} and Δv_{PV} in order to make the MPPT more adaptive [3]. However, the sensed ΔP_{PV} and Δv_{PV} are vulnerable to noises, particularly, when they are small. Therefore, an alternative method is adopted for robustness. Two points S_{PV1} and S_{PV2} on the dP_{PV}/dv_{PV} curve are selected to divide the PV operating points into three different zones. In zone 0, PV output power is close to the MPP, where a fine tracking step size is used to approach the exact MPP. In zones 1 and 2, a larger tracking step size is applied to boost up the tracking speed. The adopted MPPT algorithm is shown in Fig. 12. The tracking step sizes in zones 0, 1, and 2 are represented by $\Delta v_{ref0}, \Delta v_{ref1}$ and Δv_{ref2} respectively. K denotes the iteration number. In practice, Δv_{ref0}, Δv_{ref1}, and Δv_{ref2} are selected as 0.1, 0.3, and 0.3V, respectively. The PV voltage reference $v*pv$ is updated every 150 ms.
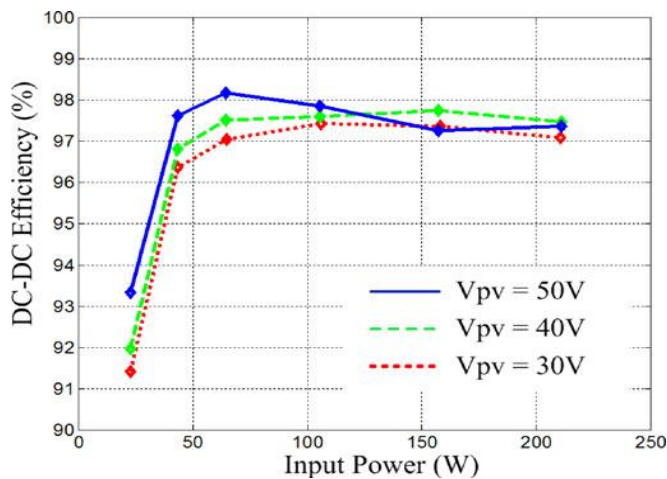
FIGURE 5: Efficiency chart of the boost-half-bridge dc–dc converter.

3. A ANFIS logic controller for MPPT

The functions of the ANFIS controller is the input of the ANFIS controller are transformed into ANFIS quantity. It supplies to the ANFIS inference system, and then ANFIS inference system will use ANFIS inference algorithm under the control of the rules of ANFIS relations, resulting in the ANFIS controller output volume. Finally, gets the accurate through anti-ANFIS to control the MPPT circuit duty cycle .ANFIS control is a non-linear essentially. It is simple to design, easy to use, strong to the anti-interference function, fast response and it has a stronger robustness to changes of the photovoltaic system. Thus ANFIS control has more advantages to other methods in the PV system. But there are also some disadvantages in the ANFIS control, such as the accuracy is not high, easy to produce oscillation and so on.

4. Structure of variable universe ANFIS control

In view of the traditional ANFIS control problems, this paper proposes using variable universe ANFIS control for maximum power point tracking. And Fig.3 shows the structure diagram of a variable universe ANFIS control system.

5. Design of variable universe ANFIS control

The inputs of the variable ANFIS controller are the error, e and one level error difference △e. The input variables are normalized using appropriate scaling factors (k_e for e and k_{ec} for △e).

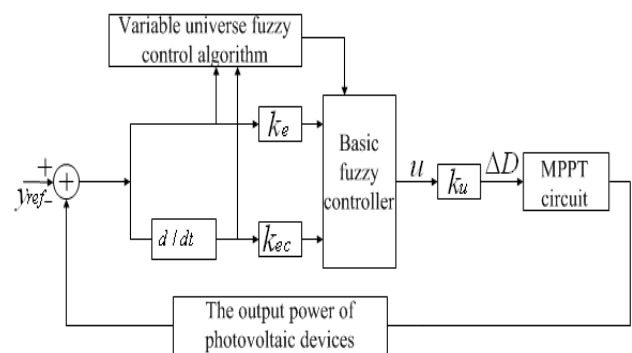
FIGURE 6: **The Structure Diagram of a Variable Universe ANFIS Control System for MPPT**

The inputs e and △e are defines as

$$e(k) = \frac{P_{pv}(K) - P_{pv}(K-1)}{V_{pv}(K) - V_{pv}(K-1)} \qquad (11)$$

$$\Delta ec(k) = e(k) - e(k-1) \qquad (12)$$

The so-called variable universe ANFIS control is to select the appropriate variable universe stretching factor. It can change the domain in place of error changes, increasing the more actual control rules. The more control points close to expectations, the smaller control class and thus can obtain a higher control precision.
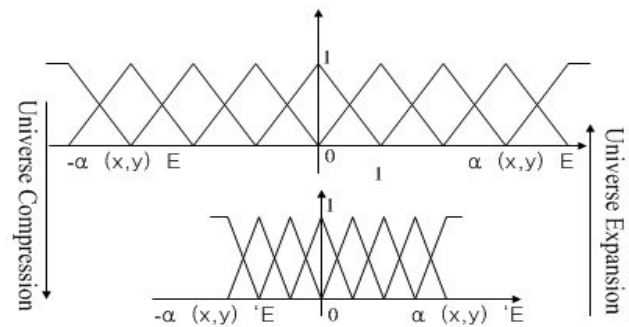

Fig.7: Variable Universe

x represents e, y represents △e. The initial domain is [-E, E]. a (x, y) is the stretching factor. The thought of the variable universe is that the shape does not change, but the universes can change with error. Thus the thought of the universe has good error adaptability. Through the stretching factor , the initial domain [-E, E] changes into [-a(x, y)*E, a (x, y) *E].

6. Design of the stretching factor

This ANFIS controller has two input variables, one output variable. a (x, ß (y) are stretching factors of these two input variables. γ (z) is the stretching factor of the output
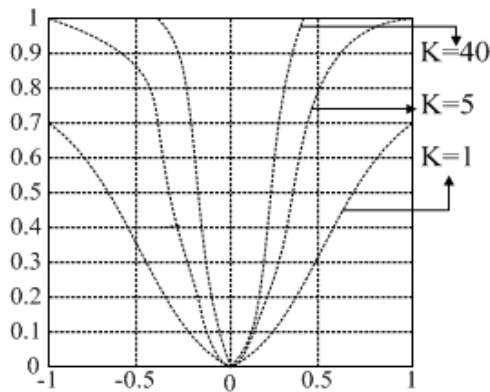
variable. Identified stretching factors are very important. The stretching factor will need to meet certain conditions：

• Duality

• a（0）=0
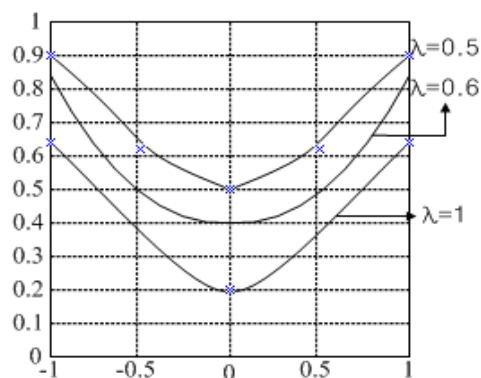
• Monotonic

• Coordination

• normality

The common used form of the stretching factor of input variable is shown as follows.

$$\alpha(x) = 1 - \lambda * e^{(-kx^2)} \, , \; \lambda \in (0,1)、 \; k \geq 0 \qquad (13)$$

The choice of λ and k has great impact on a（x）.

(a) The curve of a（x）when k changes (λ =constant)

(b) The curve of a（x） when λ changes (k=constant)

Fig.8: The curve of a（x）

We can see, the smaller is the value of a（x）, the more obvious is the compressed universe and the system response is faster.

In order to improve the system response speed, it is need to select smaller k and bigger λ . The selection method of ß（y）is the same with a（x）.

The forms of the stretching factor of output variable are shown as follows

$$\gamma(z) = K_I \sum_{i=1}^{n} P_i \int_0^l e_i(\tau)d\tau + \beta(0) \qquad (14)$$

$$\gamma(x, y) = \left[\frac{|x|}{E}\right]^{P1}\left[\frac{|y|}{EC}\right]^{P2} \qquad (15)$$

$$\gamma(x, y) = \frac{1}{2}\left[\left[\frac{|x|}{E}\right]^{P1} + \left[\frac{|y|}{EC}\right]^{P2}\right] \qquad (16)$$

It is selected a simple equation for this photovoltaic system.

$$\gamma(z) = \frac{1}{|e + 0.8|} \qquad (17)$$

F. *Simulation Results*

ANFIS controller input variables are E and EC, the output variable is duty cycle variation △D, each divided into five ANFIS sets: negative big (NB), negative small (NS), zero (ZE), and positive small (PS), positive big (PB). Input and output variables membership function is shown in Fig.6.
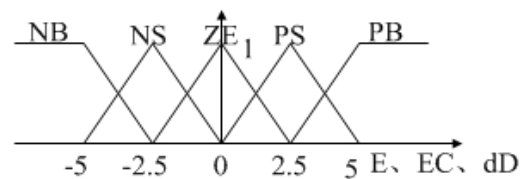

FIGURE 9: Shape of membership function and partition of ANFIS subsets for variables e, ec and △D

According to the study and experience, the ANFIS control rule base of the photovoltaic maximum power point tracking system is shown as follows in Fig.7.

EC＼E	NB	NS	ZE	PS	PB
NB	PB	PS	PS	ZE	ZE
NS	PB	PS	PS	ZE	ZE
ZE	PB	PS	ZE	NS	NB
PS	ZE	ZE	NS	NS	NB
PB	ZE	ZE	NB	NB	NB

FIGURE 10: **Rule base for the universe ANFIS control**

There is a variety of ANFIS inference algorithm, now commonly used is the Max-Min algorithm. According to FIGURE 9, it uses the following ANFIS rules IF-THEN rules to describe the knowledge of control.

$R_u^{(1)}$：If E is NB and EC is NB Then $\triangle D$ is PB

$\vdots$

$R_u^{(25)}$：If E is PB and CE is PB Then $\triangle D$ is NB

In accordance with the mathematical model of photovoltaic arrays, the simulation model of MPPT is established in the environment of Matlab/Simulink.
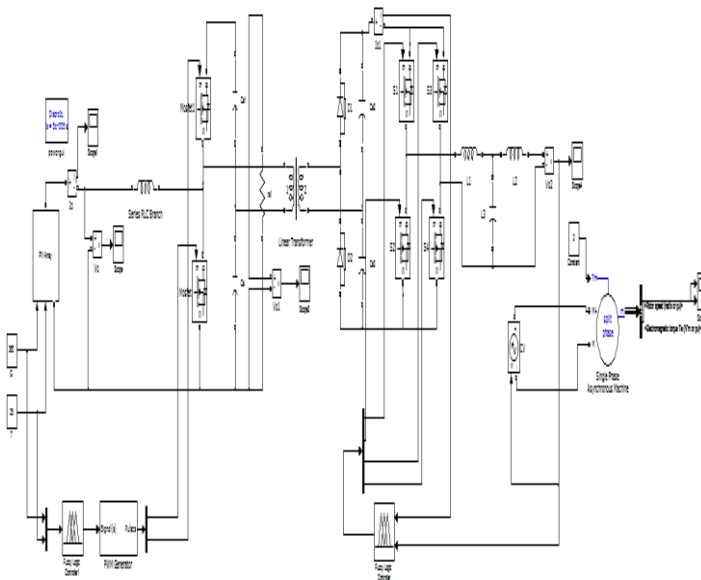
MPPT also contains a sub-model. It contains a ANFIS logic control module and an S-function to control the stretching factor of the universe ANFIS control. The quantization factor k_e and k_{ec} are divided by the corresponding stretching factor a（x）and ß（y），the scale factor k_u is multiplied by the stretching factor (z). It is shown as follows in Fig.9.
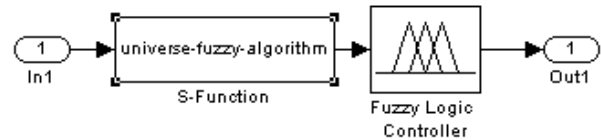

Fig.9: The sub-model of universe ANFIS control

The results of simulation of MPPT are shown in Fig.10. The variable universe ANFIS control has stronger anti-interference performance than the conventional one, and finds the maximum power point in time of 0.01 seconds. We can see that the variable universe ANFIS control can achieve higher level control precision, better speed tracking performance.
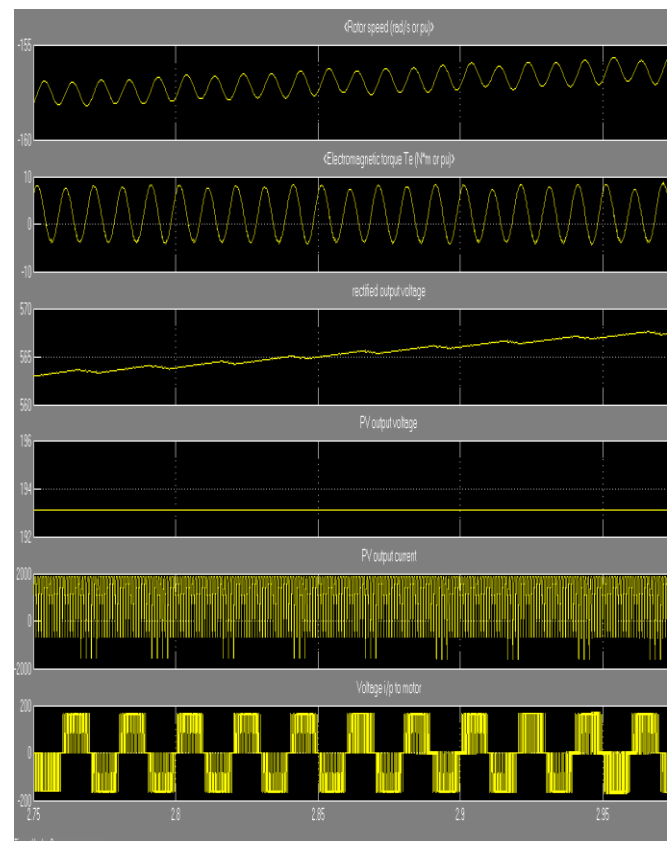

FIGURE 6.3: **Resultant waveform**

Figure 6.2: **Simulation circuit of proposed system**

G. Conclusion

A novel boost-half-bridge micro inverter for single phase induction motor connected PV systems has been presented in this paper. A plug-in repetitive current controller was proposed and illustrated. The operation principles and dynamics of the boost-half-bridge dc–dc converter were analyzed and a customized MPPT control method was developed correspondingly using ANFSI. Simulation and experimental results were shown to verify the circuit operation principles, current control, and MPPT method. Thanks to the minimal use of semiconductor devices, circuit simplicity, and easy control, the boost-half-bridge PV micro inverter possesses promising features of low cost and high reliability. According to the experimental results, high efficiency (97.0%–98.2%) is obtained with the boost-half-bridge dc–dc converter over a wide operation range. Moreover, the current injected to the single phase induction motor is regulated precisely and stiffly. High power factor (>0.99) and low THD (0.9%–2.87%) are obtained under both heavy load and light load conditions. Finally, the customized MPPT method that generates a ramp-changed reference for the PV voltage regulation guarantees a correct and reliable operation of the PV micro inverter system. The variable step-size technique provides a fast MPP tracking speed and a high MPPT efficiency (>99.7%). As a result, the proposed boost-half-bridge PV micro inverter system with its advanced control implementations will be a competitive candidate for single phase induction motor connected PV applications.

References

[1] Shuai Jiang, Dong Cao, Yuan Li and Fang Zheng Peng "Grid-Connected Boost-Half-Bridge Photovoltaic Microinverter System Using Repetitive Current Control and Maximum Power Point Tracking" IEEE Transactions On Power Electronics, Vol. 27, No. 11, November 2012.

[2] A. K. Abdelsalam, A. M. Massoud, S. Ahmed, and P. Enjeti, "High-performance adaptive perturb and observe MPPT technique for photovoltaic-based microgrids," IEEE Trans. Power. Electron., vol. 26, no. 4, pp. 1010–1021, Apr. 2011.

[3] T. Hornik and Q. C. Zhong, "A current-control strategy for voltage-source inverters in microgrids based on H∞ and repetitive control," IEEE Trans. Power Electron., vol. 26, no. 3, pp. 943–952, Mar. 2011.

[4] C. Yoon, J. Kim, and S. Choi, "Multiphase DC–DC converters using a boost-half-bridge cell for high-voltage and high-power applications," IEEE Trans. Power Electron., vol. 26, no. 2, pp. 381–388, Feb. 2011.

[5] P. C. Loh, Y. Tang, F. Blaabjerg, and P. Wang, "Mixed-frame and stationary-frame repetitive control schemes for compensating typical load and grid harmonics," IET Power Electron, vol. 4, no. 2, pp. 218–226, Feb. 2011.

[6] X. H. Wu, S. K. Panda, and J. X. Xu, "Design of a plug-in repetitive control scheme for eliminating supply-side current harmonics of three-phase PWM boost rectifier under generalized supply voltage conditions," IEEE Trans. Power Electron., vol. 25, no. 7, pp. 1800–1810, Jul. 2010.

[7] Yang Zi-Juan, Chen Yuan-Rui and Hu Jian-Ming "The Research on Application of variable Universe ANFIS Control to Maximum Power Point Tracking System" Electric Power College, South China University of Technology, Guangzhou, Guangdong and Guang Dong key laboratory of clean energy technology, 510640 Guangzhou China.

[8] Wael Labidi, Tijani Chahed and Salah-Eddine Elayoubi "Optimal battery management strategies in mobile networks powered by a smart grid" JOURNAL OF LATEX CLASS FILES, VOL. 14, NO. 8, AUGUST 2015.

[9] Fady Y. Melhem, Olivier Grunder, Zakaria Hammoudan, and Nazih Moubayed, "Energy Management in Electrical Smart Grid Environment Using Robust Optimization Algorithm" *IEEE* TRANSACTIONS ON INDUSTRY APPLICATIONS 2018.

BIOGRAPHIE

M.Gunasekaran was born in 1989 at Salem, Tamil Nadu, India. He received the Bachelor of Engineering degree in Electrical and Electronics Engineering and Master of Engineering degree in Power Electronics and Drives from Anna University (2011 & 2013) and Post Graduate Diploma degree in Internet of Things from National Institute of Electronics and Information Technology, Calicut (2017).

He is a Member of International Association of Engineers (IAENG), Lifetime Member of International Society for Research and Development (ISRD) and Associate Member (AMIE) & Chartered Engineer of Institute of Engineers India.

After few years of Industrial Experience, he is currently working as an Assistant Professor in the department of Electrical and Electronics Engineering, Annapoorana Engineering College, Salem, Tamil Nadu, India from July 2017.

His current research areas include Power Electronics and Drives, Power System, Internet of Things, Cyber security, Renewable Energy and Energy Management.